Thermal diffusivity and nonradiative relaxation rate of the $Q_1(0)+S_2(0)$ transition in solid parahydrogen measured by transient thermal lensing spectroscopy

A. Koreeda, T. Sonehara, S. Ohno, Y. Okada, and S. Saikan
Department of Physics, Graduate School of Science, Tohoku University, Sendai, 980-8578, Japan
(Received 28 June 2003; revised manuscript received 9 October 2003; published 31 December 2003)

We have measured the thermal diffusivity D_{th} and the nonradiative relaxation rates Γ for the double transitions $Q_1(0)+S_2(0)$ and $Q_2(0)+S_1(0)$ in solid parahydrogen in the temperature range from 5.2 K to 12.2 K by the technique of transient thermal lensing spectroscopy (TTLS). We have derived a formula which reproduces the temporal evolution of the TTLS signal. In this formula, we have defined a characteristic wave-vector magnitude, with which we can examine the achievement of local thermal equilibrium in the system. The characteristic wave-vector magnitude also enables quantitative comparisons between the TTLS and the transient thermal *grating* spectroscopy, which is a similar technique to the TTLS. We have obtained the temperature dependences of D_{th} and Γ by least-squares fit of the derived function to the observed signals without employing any other temperature-dependent parameters. At relatively low temperatures, the temperature dependence of D_{th} has been found to be in good agreement with that in the previous measurements, while at relatively high temperatures the values of D_{th} are slightly smaller than those in the previous measurements. We have found that Γ is almost temperature independent in the investigated temperature range as has been theoretically predicted. The value of Γ obtained is 4.3×10^4 s^{-1}, which is substantially slower than the value 3.0×10^5 s^{-1} reported by Kuo *et al.* [Phys. Rev. Lett. **53**, 2575 (1984)].

DOI: 10.1103/PhysRevB.68.224306 PACS number(s): 66.30.Xj, 33.50.Hv, 78.35.+c, 78.20.Nv

I. INTRODUCTION

Solid parahydrogen is the simplest molecular crystal and is known as a kind of quantum crystal such as solid helium. Numerous studies on solid parahydrogen have been carried out for decades in both experiments and theories, and its quantum nature has been ascribed to the weak interaction between the constituent parahydrogen molecules.[1]

In the last decade, vibrons in solid parahydrogen have been actively studied by high-resolution spectroscopy.[2–4] Furthermore, new types of nonlinear optical processes have been realized through the vibrational Raman transition $Q_1(0)$ ($v=0\rightarrow1$, $J=0\rightarrow0$).[5–7] In the nonlinear optical processes, the population and phase relaxation times of the relevant states are important factors which affect the conversion efficiency or magnitude of nonlinear susceptibility. Both relaxation times, however, have not yet been sufficiently explored in solid parahydrogen since the pioneering work of Kuo *et al.*[8]

In studying lattice anharmonicity, it is essential to know the temperature dependence of the mean free path of phonons, which can be estimated from thermal diffusivity. Although thermal properties of solid parahydrogen such as specific heat and thermal conductivity have also been explored extensively,[9,10] detailed direct measurements of the temperature dependence of the thermal diffusivity in solid parahydrogen have not been carried out so far. In addition, the temperature dependencies of the linewidth and the frequency shift for the $Q_1(0)$ transition in solid parahydrogen have been studied recently, and both the line broadening and the line shift have been ascribed to the vibron-phonon interactions.[4,11] These researches imply the necessity of further investigations on the phonon linewidth in the solid parahydrogen samples specially prepared for the optical experiments.[12] In the conventional measurements for thermal diffusivity, it is necessary to attach a heat source and temperature sensors in contact with the sample. However, it is of course more desirable to employ a nondestructive method especially for the samples used in the optical experiments as in the present case of solid parahydrogen.

In the present work, we report on the simultaneous measurement of both the thermal diffusivity and nonradiative relaxation rates for $Q_1(0)+S_2(0)$ ($v=0\rightarrow1$, $J=0\rightarrow0$; $v=0\rightarrow2$, $J=0\rightarrow2$) and $Q_2(0)+S_1(0)$ ($v=0\rightarrow2$, $J=0\rightarrow0$; $v=0\rightarrow1$, $J=0\rightarrow2$) transitions of parahydrogen molecule in solid parahydrogen by means of the transient thermal lensing spectroscopy (TTLS). For this purpose, we formulate the temporal evolution of the TTLS signal under appropriate initial and boundary conditions, and compare our formula with the conventional ones. Also a quantitative comparison between the TTLS and the transient thermal grating spectroscopy[13] (TTGS), which is a similar technique to the TTLS, is made for the first time to our knowledge. The derived formula provides simultaneous determination of the thermal diffusivity and the nonradiative relaxation rate of the parahydrogen molecule through least-squares fit to the experimental signal without employing any other temperature-dependent parameters. We also estimate the temperature dependence of the mean free path of phonons from the measured thermal diffusivity.

II. THEORY

Although there are several theories[14–16] on thermal lensing effect and the technique of TTLS, none of them matches our practical experimental arrangement. In this section, we derive a formula which reproduces the TTLS signal which is observed in our experimental arrangement.

Figure 1 is a schematic view which shows the principle of

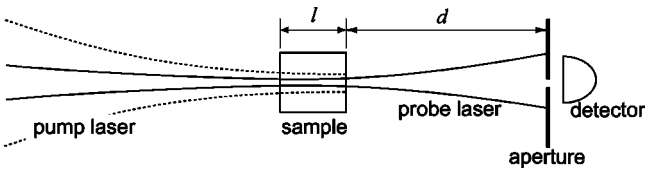

FIG. 1. A schematic view of the principle for the measurement of the TTLS signal. l and d denote the sample length and the distance between the sample and the aperture, respectively.

the measurement in the TTLS. On incident of the pulsed pump laser whose oscillating frequency is resonant to one of the transition frequencies of the hydrogen molecule, the absorbed light energy is transferred to the lattice vibrations if the transition is dipole forbidden. Therefore, an axially symmetric temperature distribution is built up in the sample at a rate which is called ''the nonradiative relaxation rate'' for the transition and then the temperature distribution decays via thermal diffusion. The above process is transferred to the cw probe laser via the optothermal lensing effect, which usually gives rise to transient defocusing of the probe beam. Thus, by monitoring the central portion of the intensity of the cw probe laser behind an aperture, we can simultaneously record both the nonradiative relaxation of the parahydrogen molecules and the thermal diffusion in solid parahydrogen in real time.

We make the following procedure to derive the time dependence of the relative signal intensity. First, by using thermodynamic theory, we derive the temporal and spatial dependences of the transient change in the refractive index, which is induced by the relaxation of the optically excited molecules. Next we derive the time dependence of the probe beam size at the position of the aperture, and finally we derive the time dependence of the relative intensity of the TTLS signal, which we detect through the aperture behind the sample.

A. Formulation for the refractive-index change

The dielectric properties of an optical medium are affected by various thermodynamic variables such as the temperature, the pressure (or stress), or the density (or strain). We assume here that the change in the refractive index includes all the contributions induced by the temperature change as

$$\delta n(\boldsymbol{r},t)=\frac{dn}{dT}\delta T(\boldsymbol{r},t), \tag{1}$$

where time- and space-dependent refractive index is defined as

$$n(\boldsymbol{r},t)=n_0+\delta n(\boldsymbol{r},t).$$

In liquids and gases, these thermal contributions to the refractive-index change are dominated by the indirect coupling between the light and heat, i.e., the refractive-index change is mainly induced by thermal expansion. In solids, especially in so-called quantum crystals which are known to have large anharmonicity, however, there may exist direct processes in which thermal fluctuations perturb dielectric constant directly.[17] We assume here that Eq. (1) contains both the direct and indirect contributions.

Assuming that $\delta n(\boldsymbol{r},t)$ is simply proportional to $\delta T(\boldsymbol{r},t)$ as in Eq. (1), all we have to do is find the analytical form of $\delta T(\boldsymbol{r},t)$ by solving thermodynamic and hydrodynamic equations. The following treatment for $\delta T(\boldsymbol{r},t)$ is partially referred to the work of Barker and Rothem.[16]

B. The thermal diffusion equation with time-dependent slow heat source

In our experiment of TTLS for solid parahydrogen, the heat source is the optically excited parahydrogen molecules. Since the transition is dipole forbidden, the absorbed light energy has to be transferred to the lattice vibrations, and raise the lattice's temperature at a rate which is called the nonradiative relaxation rate for the transition. In terms of the nonradiative relaxation rate, say Γ, we assume the time dependence of the population of the optically excited molecules as

$$N(t)=N_0e^{-\Gamma t}, \tag{2}$$

where N_0 is the initial population of the molecules in the excited state.

In most experiments for ordinary materials other than solid hydrogen, the nonradiative relaxation of molecular or electronic excitation is so fast compared to the thermal diffusion that we can usually neglect the ''buildup'' time of heat. Therefore, most conventional analyses assumed an impulsive response of the system for the heat source.[14,15] In solid hydrogen, however, the relaxation rates of the molecular excitations are expected to be much slower than those in ordinary materials due to the weak interaction between the parahydrogen molecules.[1] In addition, low temperatures of $T\lesssim 0.1\Theta_{\mathrm{D}}$, where Θ_{D} is the Debye temperature, which is 107 K for solid hydrogen, lead to relatively fast diffusion of heat. This means that in solid hydrogen the rate of thermal diffusion can increase to approach the nonradiative relaxation rate as the temperature decreases. So we must take a finite buildup time of heat into account when solving the thermal diffusion equation for solid hydrogen.

Let us first derive the inhomogeneous thermal diffusion equation to be solved. The continuity equation for the energy with a heat supply $Q(\boldsymbol{r},t)$ is

$$\frac{\partial}{\partial t}\epsilon(\boldsymbol{r},t)=-\boldsymbol{\nabla}\cdot\boldsymbol{J}(\boldsymbol{r},t)+\frac{\partial}{\partial t}Q(\boldsymbol{r},t), \tag{3}$$

where $\epsilon(\boldsymbol{r},t)$ and $\boldsymbol{J}$ are the energy and the density of the heat flux, respectively, and we have assumed an isotropic medium although solid parahydrogen has a hexagonal-close-packed structure. In terms of the mass density ρ and the specific heat (heat capacity per unit mass) C, Eq. (3) can be rewritten as

$$\rho C\frac{\partial}{\partial t}\delta T(\boldsymbol{r},t)=-\boldsymbol{\nabla}\cdot\boldsymbol{J}(\boldsymbol{r},t)+\rho C\frac{\partial}{\partial t}\Theta(\boldsymbol{r},t), \tag{4}$$

where $\Theta(\boldsymbol{r},t)$ is the temperature change caused by the heat source and we have assumed that the energy is a sum of a

constant and a fluctuating part as $\epsilon(\boldsymbol{r},t)=\epsilon_0+\delta\epsilon(\boldsymbol{r},t)$. According to Fourier's law, the heat flux density is proportional to the temperature gradient as

$$\boldsymbol{J}=-\kappa\boldsymbol{\nabla}\,\delta T(\boldsymbol{r},t), \tag{5}$$

where κ is the isotropic thermal conductivity. From Eqs. (4) and (5) we obtain the inhomogeneous thermal diffusion equation to be solved as

$$\frac{\partial}{\partial t}\delta T(\boldsymbol{r},t)-D_{\rm th}\nabla^2\delta T(\boldsymbol{r},t)=\frac{\partial}{\partial t}\Theta(\boldsymbol{r},t), \tag{6}$$

where the isotropic thermal diffusivity has been introduced as

$$D_{\rm th}=\frac{\kappa}{\rho C}. \tag{7}$$

Since no temperature change exists at $t=0$ and our sample has a cylindrical shape, we set the initial and boundary conditions for Eq. (6) as

$$\delta T(r,\theta,z,0)=0,$$

$$\delta T(R,\theta,z,t)=0,$$

respectively, where we have adopted cylindrical coordinates, namely, $\boldsymbol{r}=(r,\theta,z)$, and R is the radius of the cylindrical sample cell. In our experiment, C has to be C_V (specific heat at constant volume) because our sample is not allowed to expand or shrink in the cell[12] as will be mentioned in Sec. III.

Let us now find the explicit form of $\Theta(\boldsymbol{r},t)$. Let $q_{\rm mol}$ be the absorbed energy of one molecule and $f(\boldsymbol{r})$ be the spatial distribution of the excited molecules, then $Q(\boldsymbol{r},t)$ can be expressed as

$$Q(\boldsymbol{r},t)=q_{\rm mol}[N_0-N(t)]f(\boldsymbol{r},t),$$

where $N(t)$ is assumed to have the form defined in Eq. (2). Since the absorption coefficient α can be expressed as $\alpha=N_0q_{\rm mol}/Q_0$, where Q_0 is the incident pulse energy of the pump laser, $\Theta(\boldsymbol{r},t)$ can be written as

$$\Theta(\boldsymbol{r},t)=\frac{\alpha Q_0}{\rho C_V}(1-e^{-\Gamma t})f(\boldsymbol{r}).$$

If the pump laser has a Gaussian beam profile whose beam radius is w, the spatial distribution of the excited molecules can be written as $f(\boldsymbol{r})=e^{-2r^2/w^2}$ and the heat source term, namely, the right-hand side of Eq. (6) can be expressed as

$$\frac{\partial}{\partial t}\Theta(\boldsymbol{r},t)=\frac{\alpha Q_0\Gamma}{\rho C_V}e^{-\Gamma t}e^{-2r^2/w^2}. \tag{8}$$

We can expand the spatial part (the Gaussian distribution) in the inhomogeneous term, Eq. (8), by the Bessel function of order zero, which is the eigenfunction of the homogeneous version of Eq. (6) as follows:

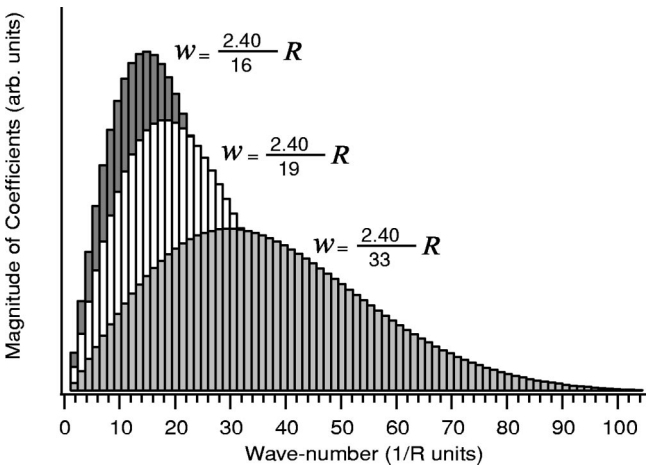

FIG. 2. Magnitudes of the expansion coefficients c_n for various pump beam radii. From the upper trace $w=(2.40/16)R$, $(2.40/19)R$, and $(2.40/33)R$, respectively. Note that the largest contributions are located at $q_n\simeq 2.40/w=\overline{q}$, i.e., at $q_n=16/R$, $19/R$, and $33/R$.

$$e^{-2r^2/w^2}=\sum_{n=1}^{\infty}c_nJ_0(q_nr), \tag{9}$$

where q_n is the nth eigenvalue and can be expressed as $q_n=\lambda_n/R$, with λ_n the nth zero of $J_0(x)$, namely, $\lambda_1=2.40$, $\lambda_2=5.52$, $\lambda_3=8.65$, and so on. The expansion coefficient c_n can be expressed in terms of orthogonality for the Bessel function as

$$c_n=\frac{2}{J_1^2(q_nR)}\int_0^R re^{-2r^2/w^2}J_0(q_nr)dr,$$

where $J_1(x)$ is the Bessel function of order one. Note that c_n is a function of w and R, and that the smaller w gives more contributions of large q_n's when R is fixed. This means that reducing the pump-beam radius increases the number of the modes which diffuse relatively fast. Figure 2 shows the magnitudes of c_n's for different values of w. It is seen that the largest contributions are located at $q_n\simeq\lambda_1/w$. Therefore, we may define a characteristic wave-vector magnitude in the TTLS as

$$\overline{q}\simeq\frac{\lambda_1}{w}=\frac{2.40}{w}. \tag{10}$$

The characteristic wave-vector magnitude $\overline{q}$ enables a quantitative comparison between the TTLS and TTGS.[13] In the TTGS, the magnitude of the induced wave vector is explicitly expressed as

$$q=2n\frac{2\pi}{\lambda_{\rm pump}}\sin\frac{\theta}{2}, \tag{11}$$

where $\lambda_{\rm pump}$ and θ are the wavelength of the pump light and the intersecting angle between the two pump beams, respectively. Thus, we have an approximate relation between w in the TTLS and θ in the TTGS as

$$\theta w \simeq 0.38 \frac{\lambda_{\text{pump}}}{n}, \tag{12}$$

where θ is assumed to be small. This relation shows, for example, that for $\lambda_{\text{pump}}=800$ nm and $n=1.14$ an intersecting angle of 10 mrad in the TTGS approximately corresponds to a pumping-beam radius of 27 μm in the TTLS. Equation (12) is particularly useful in determining the practical experimental arrangements in the TTLS if the mean free path of phonons has to be taken into account.

If we assume that $\delta T(r,t)$ can be separated into temporal and spatial part as

$$\delta T(r,t) = \frac{\alpha Q_0 \Gamma}{\rho C_V} \sum_{n=1}^{\infty} \mathcal{T}_n(t) J_0(q_n r), \tag{13}$$

and substituting Eqs. (9) and (13) into Eq. (6), we obtain the temporal part $\mathcal{T}_n(t)$ as follows:

$$\mathcal{T}_n(t) = \frac{c_n}{\Gamma - D_{\text{th}} q_n^2} (e^{-D_{\text{th}} q_n^2 t} - e^{-\Gamma t}). \tag{14}$$

Note that the sign of $\mathcal{T}_n(t)$ does not change regardless of whether $D_{\text{th}} q_n^2$ is greater or less than Γ. Furthermore, $\mathcal{T}_n(t)$ does not diverge even when $D_{\text{th}} q_n^2 \to \Gamma$ because

$$\lim_{D_{\text{th}} q_n^2 \to \Gamma} \mathcal{T}_n(t) = c_n t e^{-\Gamma t}.$$

Substituting Eq. (14) into Eq. (13), we obtain a solution for Eq. (6) as

$$\delta T(r,t) = \frac{\alpha Q_0 \Gamma}{\rho C_V} \sum_{n=1}^{\infty} \frac{c_n}{\Gamma - D_{\text{th}} q_n^2} (e^{-D_{\text{th}} q_n^2 t} - e^{-\Gamma t}) J_0(q_n r). \tag{15}$$

It should be noted that we will observe multiple wave-vector components of the temperature change through diffraction of the probe laser rather than observe only one wave-vector component as in the TTGS or spontaneous Rayleigh light scattering experiments: in other words, we can regard Eq. (15) as a superposition of the solutions with various wave-vector magnitudes in the TTGS or spontaneous Rayleigh light scattering. Figure 3 shows the temporal and spatial dependences of the solution, Eq. (15). It is seen that the spatial width of the initial Gaussian distribution broadens as time goes on.

As a comparison with the previous theories,[8,14,15,18] we consider a characteristic time with which heat diffuses. The characteristic time t_c adopted by Kuo *et al.* was $w^2/8D_{\text{th}}$,[8] while that in our case is $(D_{\text{th}}\overline{q^2})^{-1} = w^2/5.78 D_{\text{th}}$, which is comparable to the former and indicates that $\overline{q}$ consistently represents the average wave vector in the TTLS of our experimental arrangement. The different factors 1/8 and 1/5.78 in the two cases probably arise from the different boundary conditions: $R \to \infty$ was assumed in the former, while a finite R is assumed in our case.

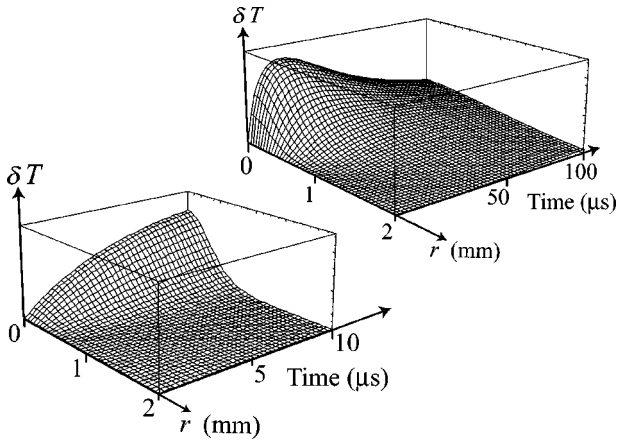

FIG. 3. The spatial and time evolution of the solution for Eq. (6): (a) $0 \leqslant t \leqslant 10$ μs; (b) $0 \leqslant t \leqslant 100$ μs. The values employed for w, D_{th}, and Γ are 250 μm, 2×10^{-2} m^2/s, and 5×10^4 s^{-1}, respectively.

C. The time-dependent signal intensity

In the TTLS experiment, a central portion of the probe beam intensity is monitored through an aperture. According to Ref. 15, the spot radius of the probe laser at the position of the aperture is given as

$$\omega_3^2(t) = \frac{\lambda}{\pi b}\left[\left(1 - \frac{d}{f(t)}\right)^2 b^2 + (l+d)^2\right], \tag{16}$$

where λ is the wavelength of the probe laser, $b \equiv \pi\omega_1^2/\lambda$ is the Rayleigh length (or the confocal parameter), and ω_1 is the spot radius of the probe laser at $z=0$, i.e., at the front surface of the sample. $f(t)$ is the time-dependent effective focal length of the medium which is associated with the temperature distribution as[14]

$$\frac{1}{f(t)} = l \frac{dn}{dT} \frac{\partial^2}{\partial r^2} \delta T(r,t)\big|_{r=0}. \tag{17}$$

Substituting Eq. (15) into Eq. (17), Eq. (16) becomes

$$\omega_3^2(t) = \frac{\lambda}{\pi b}\left[\left(1 - ld\frac{dn}{dT}\delta T''(0,t)\right)^2 b^2 + (l+d)^2\right], \tag{18}$$

where

$$\begin{aligned}\delta T''(0,t) &= \frac{\partial^2}{\partial r^2}\delta T(r,t)\big|_{r=0} \\ &= \frac{\alpha Q_0 \Gamma}{\rho C_V} \lim_{r\to 0} \sum_{n=1}^{\infty} q_n^2 \mathcal{T}_n(t) \frac{1}{2}[J_2(q_n r) - J_0(q_n r)] \\ &= -\frac{1}{2}\frac{\alpha Q_0 \Gamma}{\rho C_V} \sum_{n=1}^{\infty} q_n^2 \mathcal{T}_n(t).\end{aligned} \tag{19}$$

Here $\mathcal{T}_n(t)$ and $\delta T(r,t)$ are defined in Eq. (14) and Eq. (15), respectively, and $J_2(x)$ is the Bessel function of order 2.

For a Gaussian-beam profile with a spot radius of $\omega_3(t)$, the normalized intensity $\mathcal{I}(t)$ detected behind an aperture of radius a is given as

$$\mathcal{I}(t;a)=\frac{I(t;a)}{I(t;a)|_{a\to\infty}},$$

where $I(t;a)$ is the probe-beam intensity detected behind an aperture of radius a, and $I(t;a)|_{a\to\infty}$ is the total probe-beam intensity at the position of the aperture. Since $I(t;a)$ can be calculated as

$$I(t;a)=I_0\int_0^a dr\int_0^{2\pi} d\theta r e^{-2r^2/\omega_3^2(t)}$$

$$=\frac{\pi}{2}I_0\omega_3^2(t)[1-e^{-2a^2/\omega_3^2(t)}],$$

$\mathcal{I}(t;a)$ can be written as

$$\mathcal{I}(t;a)=1-e^{-2a^2/\omega_3^2(t)}.$$

Following the conventional formulations[14–16] for the time-dependent signal intensity, we adopt the change in the intensity ratio relative to the initial value, i.e.,

$$S(t;a)=1-\frac{\mathcal{I}(t;a)}{\mathcal{I}(0;a)}=1-\frac{1-e^{-2a^2/\omega_3^2(t)}}{1-e^{-2a^2/\omega_{30}^2}},\qquad(20)$$

where $\omega_{30}=\omega_3(0)$, which is defined in terms of Eqs.(16) and (17) as

$$\omega_{30}^2=\frac{\lambda}{\pi b}[b^2+(l+d)^2].$$

For a small a and a large ω_3, Eq. (20) can be approximated through series expansion of the exponential functions as

$$S(t)\simeq 1-\frac{\omega_{30}^2}{\omega_3^2(t)},\qquad(21)$$

and becomes independent of the aperture radius a. Equation (21) is consistent with the previous analyses,[8,15] which assume that the intensity behind the aperture is inversely proportional to the spot area of the probe beam. This is exactly correct only for a probe beam with a uniform spatial distribution of intensity. As we will mention below, however, since $a=1.5$ mm and $\omega_{30}=4.6$ mm in our experiment, $2a^2/\omega_3^2$ becomes as large as 0.21, which implies that the approximation using Eq. (21) is not relevant in our analysis.

Substituting Eq. (18) into Eq. (20), we obtain a theoretical signal intensity as a function of $\delta T''(0,t)$ of Eq. (19), and we can numerically trace it. However, it is more straightforward to trace the theoretical signal as a function of temperature change δT rather than $\delta T''(0,t)$ itself. To do so, we assume in Eq. (19) that $\delta T''=-\frac{1}{2}\overline{q}^2\delta T_{\rm eff}$, where $\overline{q}$ is the magnitude of an average wave vector which was defined in Eq. (10) and $\delta T_{\rm eff}$ is the effective temperature change during the transient thermal lensing effect. The theoretical trace of the normalized signal intensity against $\delta T_{\rm eff}$ is shown in Fig. 4. The parameters employed are approximately equal to those we have adopted in our experiment; $l=1$ cm, $d=3$ m, $\lambda=514.5$ nm, $b=15$ cm, $n_0=1.14$, $w=470$ μm, and $dn/dT=-2\times10^{-4}$ K^{-1}. The value of dn/dT is about three times larger than that used by Kuo *et al.* in Ref. 8 in accordance with the analysis made by Li *et al.*[19] The inset shows the same curve in the range of $0\leqslant\delta T<1$ K. Naturally, the normalized signal intensity is saturated for a sufficiently large temperature change.

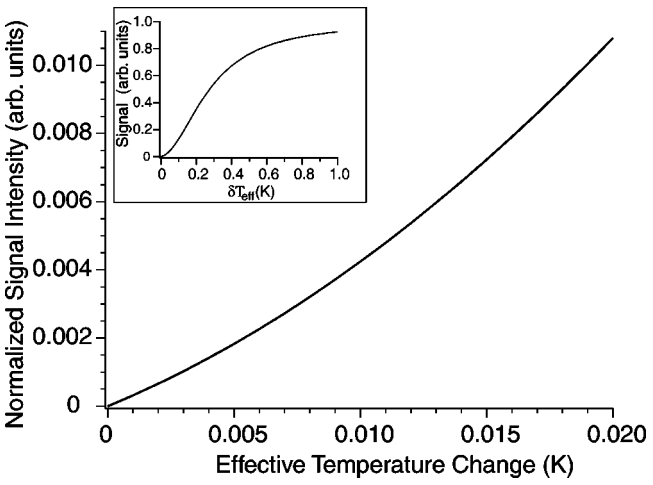

FIG. 4. Normalized theoretical signal intensity as a function of the effective temperature change in the range of $0\leqslant\delta T_{\rm eff}<0.02$ K. The inset shows the same curve in the range of $0\leqslant\delta T_{\rm eff}<1$ K. It is important to note that we have deduced the effective temperature change $\delta T_{\rm eff}$ by assuming an average wave vector of $\overline{q}=\lambda_1/w$, where $\lambda_1=2.40$. The values of the parameters employed in this simulation are presented in the text.

It is found in Fig. 4 that the signal intensity can be roughly regarded as a linear function of $\delta T_{\rm eff}$ or $\delta T''(0,t)$ if $S(t;a)$ is as small as 0.01. This means that the expression for $\delta T''(0,t)$ of Eq. (19) can directly reproduce the experimental signals if the experiments are so performed that the relative signal intensity does not exceed 0.01. This makes it quite simple to estimate both the thermal diffusivity and the nonradiative decay rate simultaneously in the TTLS, despite the fact that the rigorous time dependence of the signal intensity, which is given in Eq. (20) in terms of Eq. (18), has a rather complicated form. The difference between a linear function and the curve shown in Fig. 4 critically depends on the magnitudes of the coefficients which are multiplying $\delta T''(0,t)$ in Eq. (18). In the simulation made above, the relative difference is less than 15%, which is reasonably accurate in our analysis regarding the temporal fluctuations in the experimental signal intensity, which are typically 10% or greater.

To check the actual effect of the nonlinearity described above, we have measured the pump-energy dependence of the signal intensity of the TTLS. However, we could not find any distinguishable nonlinearity within the experimental errors, i.e., we found that the signal intensity was almost proportional to the temperature change within the experimental errors. Although there remains a possibility of overestimation of the nonlinearity in the simulation, the result indicates that Eq. (19) can actually reproduce the experimental signal

and also ensures a simple analysis of the experimental data. Therefore, we can conclude that the time dependence of the signal intensity of the TTLS in our experimental arrangement can be expressed quite simply as

$$S(t)=A\sum_{n=1}^{\infty} q_n^2\mathcal{T}_n(t), \tag{22}$$

where A is a proportionality coefficient.

III. EXPERIMENT

We used the TTLS method to measure the temperature dependence of the thermal diffusivity and nonradiative relaxation in solid parahydrogen. The principle of this method has been already mentioned in the beginning of Sec. II. It is, however, well known that the TTGS (Ref. 13) is more advantageous than the TTLS, in that the TTGS can explicitly define the wave vector of the observed excitation. So, we should comment here on the reasons why we did not choose the TTGS but the TTLS.

In the TTGS, the intersecting angle between the two pump beams has to be smaller than a few mrad for the present sample of solid parahydrogen because q defined in Eq. (11) has to be as small as possible in order that local thermal equilibrium is always achieved, as will be discussed later in Sec. IV D. Such a small intersecting angle makes it difficult to distinguish the true signal from the parasitic background of the strong thermal lensing effect. Furthermore, the situation becomes more difficult if we prepare a purer parahydrogen sample because higher parahydrogen concentration makes the thermal diffusion faster and requires a still smaller intersecting angle. In fact, we could not obtain any reproducible signals in the TTGS for solid parahydrogen.

In the TTLS, however, such a condition for the achievement of local thermal equilibrium can be easily satisfied by adopting a pumping-beam radius larger than $\approx 100\ \mu$m, which we can estimate from Eq. (12). That is why we decided to adopt the TTLS rather than the TTGS from the viewpoint of experimental reliability.

A. Experimental setup for the TTLS

The experimental setup for the TTLS is depicted in Fig. 5. The pump laser was a pulsed-tunable Littman-type Ti:sapphire laser pumped by the second harmonic of a Nd:YAG (yttrium-aluminum-garnet) laser whose pulse width was ≈ 7 nsec. The probe laser was a cw Ar^+ laser oscillating at a single longitudinal mode of 514.5 nm. In order to avoid sample heating by the probe laser, an acousto-optic modulator was inserted for reduction of duty. The pump and probe beams collinearly entered into the sample, and only the probe beam was filtered by a short-wave pass filter. A grating was placed after the short-wave pass filter in order to reject the residual pump laser. The aperture before the detector transmitted the central portion of the probe beam. The spot sizes of the pump and probe beams were individually varied by changing each of the focusing lenses. To ensure uniform defocusing effects in the pump region, the focal lengths of the focusing lenses were carefully chosen so that the spot

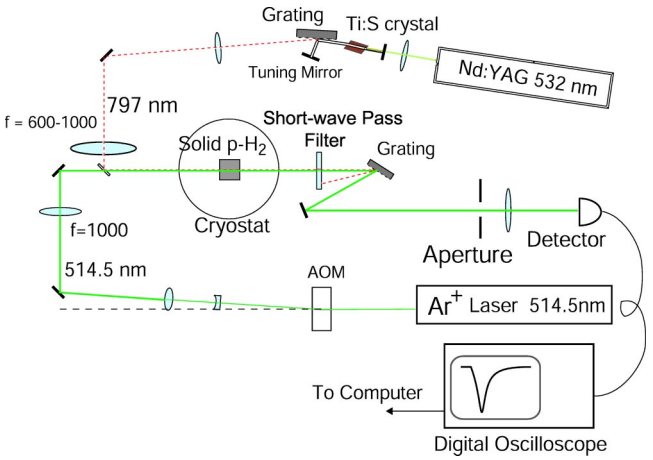

FIG. 5. (Color online) Experimental setup for the transient thermal lensing spectroscopy. The short-wave pass filter and grating are placed for rejection of the pump laser.

size of the probe laser became smaller than 1/3 of that of the pump laser. The Rayleigh length b of the probe laser was $\approx 10-15$ cm, and the spot radius at the aperture in the absence of the pump laser, namely, ω_{30}, was 4.6 mm. The spot radius of the pump laser at the sample surface was 470 μm. The Rayleigh length and the spot sizes were measured by using a 12-mm-long linear charge-coupled device array, and both the pump and probe beams were found to have a well-defined Gaussian spatial profiles. The distance from the sample to the aperture d was 2.92 m. The temporal change of the probe-beam intensity was recorded by a digital oscilloscope and was averaged over 100 to 300 times by a computer.

B. Sample preparation

The solid parahydrogen sample was prepared by means of liquid-phase pressurizing method,[12] which can provide transparent and crack-free single crystals of parahydrogen. Furthermore, parahydrogen crystals grown by this method have a high damage threshold against incident pulse lasers. The sample cell was made of 10-mm-thick stainless steel and had a 10-mm-diameter hole for the sample and a 1-mm-thick Teflon cylindrical spacer. Therefore, the sample crystal had an 8 mm diameter and 10 mm thickness. The ortho-para conversion was carried out at temperatures between 15 K and 17 K, providing a parahydrogen concentration of 99.7%, which we measured from the integrated intensity ratio between the spontaneous Raman scattering lines for $S_0(0)$ ($J=0\rightarrow 2$, $v=0\rightarrow 0$) and $S_0(1)$ ($J=1\rightarrow 3$, $v=0\rightarrow 0$).[20]

In the TTLS, it is necessary to deposit heat in the sample. In our experiments, we made use of the nonradiative relaxation of rotational-vibrational excited states of parahydrogen molecule, namely, $Q_1(0)+S_2(0)$ and $Q_2(0)+S_1(0)$. Figure 6 shows the absorption spectrum of the $Q_1(0)+S_2(0)$ and $Q_2(0)+S_1(0)$. These *double transitions* are known to occur via induced dipole moments due to molecular quadrupolar and higher-order induction mechanisms: since the induced dipole moment is a consequence of interactions of a pair of molecules, simultaneous transitions of two molecules upon

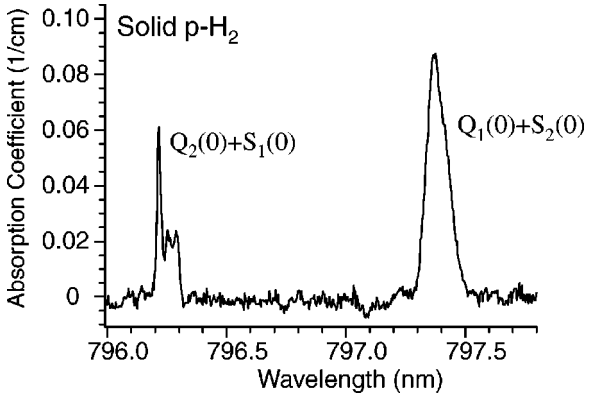

FIG. 6. Absorption coefficient of solid parahydrogen in the wavelength range from 796 nm to 798 nm. The absorbing band in the right arises from the $Q_1(0)+S_2(0)$ transition, while the band in the left from the $Q_2(0)+S_1(0)$ transition.

absorption of one radiation quantum can be observed.[1,21] The pulsed Ti:sapphire laser was tuned to each of the absorption lines by monitoring the TTLS signal. The excitation energy was carefully reduced so as not to excite any $Q_1(0)$ transition via stimulated Raman scattering, which could give rise to a TTLS signal due to the nonradiative relaxation of the $Q_1(0)$ transition.[19]

We observed the TTLS signals for both the $Q_1(0)+S_2(0)$ and $Q_2(0)+S_1(0)$ transitions and found that the signal intensity was stronger for the $Q_1(0)+S_2(0)$ transition. However, we could not find any significant difference in both the rising and decay rates of the TTLS signals for the two transitions within the experimental error. Therefore, we will mention only the results for the $Q_1(0)+S_2(0)$ transition hereafter.

IV. EXPERIMENTAL RESULTS AND DISCUSSION

A. Temperature dependence of the TTLS signals and the fitting results

The temperature dependence of the TTLS signals is shown in Figs. 7(a) and 7(b), where the open and solid circles represent the experimental signals and the solid curves are the least-squares fit of Eq. (22). A slow rising behavior is clearly seen in Fig. 7(a) indicating a slow nonradiative relaxation of H_2 molecules in solid parahydrogen. Also we see in Fig. 7(b) that the signal decay due to thermal diffusion becomes faster with decreasing temperature.

As seen in Fig. 7(a), at relatively high temperatures, namely, $T \gtrsim 10$ K, the heat diffuses so slow compared to the temperature rising rate that one may ignore the effect of thermal diffusion in a sufficiently short time after pumping. In such a case, the nonradiative relaxation rate for the molecules can be determined by least-squares fit of a single exponential growth function as

$$S(t) \propto 1 - e^{-\Gamma t}, \tag{23}$$

to the signal rising region. This is because Eq. (22) becomes proportional to $1-e^{-\Gamma t}$ as D_{th} goes to zero. In fact, we were able to fit Eq. (23) to the data for 11.2 K and 12.2 K successfully with two additional fitting parameters, namely, a scaling factor and baseline. It should be noted, however, that the approximation by Eq. (23) is only valid when $\Gamma \gg D_{\mathrm{th}}\overline{q^2}$: if heat diffuses faster than it is created, then the signal does not build up at a rate of Γ but builds up approximately at a rate of $D_{\mathrm{th}}\overline{q^2}$ as will be discussed in Sec. IV E.

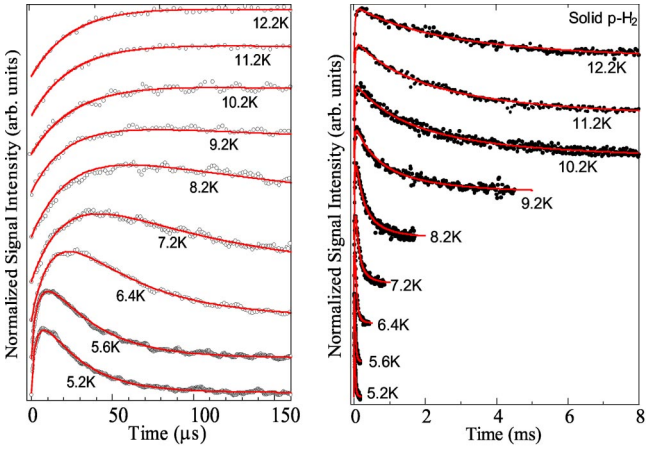

(a) $0 \le t \le 150$ μs (b) $0 \le t \le 8$ ms

FIG. 7. (Color online) Temperature dependence of the TTLS signal for solid parahydrogen in the temperature range from 5.2 K to 12.2 K. (a) $0 \leqslant t \leqslant 150$ μs, (b) $0 \leqslant t \leqslant 8$ ms. The solid curves are the least-squares fits of Eq. (22) to the experimental data. Note that each trace is normalized at its peak intensity.

In order to obtain the nonradiative decay rate only, there is another simple way of approximation for the signal rising region: only the initial slope of the signal at $t \simeq 0$ has been measured in Refs. 8 and 19. The initial slope of Eq. (20) is given as

$$\left.\frac{d}{dt}S(t;a)\right|_{t=0} = (e^{2a^2/\omega_{30}^2}-1)^{-1}\frac{16a^2b^2ld}{[b^2+(l+d)^2]^2w^2}\left|\frac{dn}{dT}\right|\frac{\alpha Q_0}{\rho C_V}\Gamma, \tag{24}$$

where we have assumed that dn/dT is negative and have used a relation for Eq. (19) that

$$\lim_{r\to 0}\left[\lim_{t\to 0}\frac{d}{dt}\delta T''(r,t)\right] = -\frac{\alpha Q_0}{\rho C_V}\frac{4}{w^2}\Gamma.$$

Since Eq. (24) is proportional to Γ, one can experimentally measure Γ only from Eq. (24) in principle. It is important to note that the initial slope of the signal of Eq. (24) does not depend on the rate of the thermal diffusion. Therefore, although it has not been discussed before, this approximation can be applied for signals even at relatively low temperatures, where thermal diffusion rate is comparable to or even faster than the buildup of heat by nonradiative relaxation of the molecules.

Recently, Li *et al.*[19] have investigated very carefully the temperature dependence of Γ for the $Q_1(0)$ transition of

solid parahydrogen utilizing Eq. (6) of Ref. 8, which is essentially equivalent to Eq. (24). For its sake, however, one must accurately know all the 11 parameters on the right-hand side of Eq. (24). The parameters include not only the geometrical parameters which require very careful measurements but also the temperature-dependent variables such as α, ρ, C_V, or dn/dT, some of which are strongly sample dependent or not fully given in tables. Furthermore, it is of course impossible to obtain the thermal diffusivity in this way.

In contrast, the least-squares fit of Eq. (22) to the entire data points completely eliminate the above difficulty since the initial slope, i.e., the scaling factor, is just a fitting parameter in this case. In fact, we set only four fitting parameters in our analysis, namely, the scaling factor, the baseline Γ, and D_{th}. We first found the initial values for D_{th} and Γ by fit of an approximate function as

$$S(t)=A(e^{-\Gamma t}-e^{-D_{\mathrm{th}}\bar{q}^2 t})+B, \tag{25}$$

where A and B are the scaling factor and baseline, respectively. Since Eq. (25) can be regarded as a single-component version of Eq. (22), one can obtain an approximate value of Γ and D_{th}.

We took 32 terms in the sum in Eq. (22), which was found to be accurate enough for our experimental arrangement. While we could fit Eq. (22) to the entire data points in the signals at 11.2 K and 12.2 K, better fitting results were obtained when we fitted Eq. (22) and Eq. (23), respectively, to the signal decay and rising region of these high-temperature data. This is probably due to the fact that the number of the data points in the signal rising region for such high temperatures is much fewer than that in the decay region as seen in Fig. 7(b).

As the temperature is lowered, the thermal diffusion becomes faster as seen in Fig. 7(b). At temperatures below 10 K, Eq. (22) almost completely reproduces the entire experimental points, while the approximation by Eq. (23) for the signal rising region described above is invalid in this temperature region since the rising and decay regions can no longer be separated as done at higher temperatures.

In the subsequent sections, we will present the temperature dependences of the nonradiative decay rate for $Q_1(0)+S_2(0)$ transition and the thermal diffusivity in solid parahydrogen, and make some discussions on them.

B. Temperature dependence of Γ

The temperature dependence of the nonradiative relaxation rate for $Q_1(0)+S_2(0)$ transition is shown in Fig. 8. The open squares (□) represent the values which were obtained by fitting Eq. (22) to the entire data points of each signal trace, while the open triangles (△) and the solid circles (●) were obtained by fitting Eq. (22) and Eq. (23), respectively, to the rising part of the signal.

The value which was obtained at 11 K by Kuo *et al.*[8] is 3.0×10^5 s^{-1}, and it is approximately seven times larger than our value at nearly the same temperature. As mentioned in Ref. 19, the large difference might come from the $|dn/dT|$ value employed by Kuo *et al.*, which was about three times

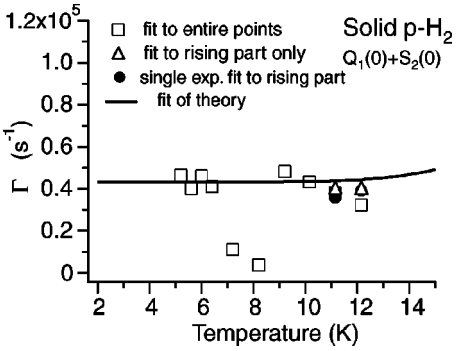

FIG. 8. The temperature dependence of the nonradiative relaxation rate for $Q_1(0)+S_2(0)$ transition in solid parahydrogen. The open squares represent the values obtained by fitting Eq. (22) to the entire data points. The open triangles and solid circles are the values obtained by fitting Eq. (22) and Eq. (23), respectively, to the signal rising part only. The solid curve is obtained by fitting Eq. (26) to the best-fit values for the measured Γ with one fitting parameter Γ_0.

smaller than that employed by Li *et al.*, yielding a three times faster Γ in accordance with Eq. (24). Even if we take this into account, the value 1.0×10^{-5} s^{-1} by Kuo *et al.* is still more than twice as fast as ours. There might be some other possible reasons, e.g., the different way of sample preparation or the different orthohydrogen concentration, but this difference in the value of Γ is probably due to the uncertainty in other parameters such as dn/dT in Eq. (24) which they used in their analysis. In contrast, no parameter is necessary to be known in our analysis.

The values obtained for Γ are almost temperature independent in the temperature range investigated except the two values at 7.2 K and 8.2 K. As we will discuss later in Sec. IV E, these two values are probably due to an artifact in the process of the least-squares fit of Eq. (22); the fitting program seems to become unstable around 7 K because it encounters some $\frac{0}{0}$ problem due to the coincidence of the rate of thermal diffusion and the rate of nonradiative relaxation around 7 K.

There is a theory[22–24] which accounts for the temperature dependence of the nonradiative relaxation in molecular crystals in terms of the multiphonon processes, and it predicts a very weak temperature dependence at low temperatures. A quantitative comparison of our result with the theory requires some unavailable parameters such as the average vibron frequency or the most probable number of vibrons involved in the relaxation processes. Instead, however, a simpler case in which the molecule is embedded in a monatomic lattice can be compared to the experimental result as a reference. The temperature dependence of the nonradiative relaxation in this case of monatomic lattice is predicted to be appreciably stronger than in the case of such a polyatomic lattice as solid parahydrogen.[23] The solid curve in Fig. 8 is a fit of the theoretical function of Eq. (30) in Ref. 23 with only one fitting parameter, the relaxation rate at $T=0$ K. It is predicted that the onset of the temperature dependence appearing $T\gtrsim12$ K in Fig. 8 should shift to the higher temperatures and the temperature coefficient of Γ should be much smaller for the case of a polyatomic lattice.[23] We have assumed that the nonradiative relaxation rates are additive and have the form

$$\Gamma(T)=\tfrac{1}{3}\Gamma_0[g_1(T)+2g_2(T)], \tag{26}$$

according to the discussions by Kuo *et al.*[8] Here Γ_0 is the nonradiative relaxation rate at $T=0$ K; $g_1(T)$ and $g_2(T)$ are the normalized nonradiative relaxation rates for $v=1$ and $v=2$ vibrational excited states, respectively, and their explicit form is[23]

$$g_v(T)=(e^{\hbar\omega_v/k_BT}-1)(e^{\hbar\omega_A/k_BT}-1)^{-\omega_v/\omega_A},$$

where ω_v and ω_A are the vibrational frequency of the molecule for the vth vibrational excited state and the average lattice phonon frequency, respectively. We have assumed that $\omega_{v=1}=4150$ cm^{-1} and $\omega_{v=2}=2\omega_{v=1}=8300$ cm^{-1}, which satisfy that $\omega_{v=1}+\omega_{v=2}\simeq 12\,500$ cm^{-1}, the measured frequency of the $Q_1(0)+S_2(0)$ transition as described in Sec. III B. Also we have assumed that the average lattice phonon frequency corresponds to the Debye frequency of solid hydrogen, i.e, $\omega_A=70$ cm^{-1}.[10] The value of Γ_0 obtained by fitting Eq. (26) was 4.3×10^4 s^{-1}, which almost coincides with the average of the measured values of Γ except the data points at 7.2 K and 8.2 K. Taking the predicted weaker temperature dependence into account, we can conclude that Γ is almost constant at least in the temperature range investigated, and the value is 4.3×10^4 s^{-1}. This result will be referred in the analysis for $D_{\rm th}$ later in Sec. IV C.

Recently, Li *et al.* have made another quantitative comparison between the theory and experiment for the temperature dependence of the nonradiative relaxation in solid parahydrogen for $Q_1(0)$ transition.[19] They reported that they could not reproduce the increasing behavior of the observed temperature dependence of $\Gamma_{Q1(0)}$ if they set $\omega_A=70$ cm^{-1}, which is the Debye frequency of solid hydrogen, while they could if they assumed that $\omega_A=40$ cm^{-1}. The difference between the analysis made by Li *et al.* and ours might come from the different excited states investigated, namely, $Q_1(0)$ and $Q_1(0)+S_2(0)$, or it might come from the different excitation method, i.e., the use of stimulated Raman scattering and optical absorption. However, since they utilized a formula like Eq. (24), it is also possible that the uncertainties in some of the temperature-dependent parameters employed in the formula would be significant.

C. Temperature dependence of $D_{\rm th}$

The temperature dependence of the thermal diffusivity of the solid parahydrogen is shown in Fig. 9. The measured thermal diffusivity increases with decreasing temperature. In Fig. 9, the closed circles (●) represent the values obtained by fitting Eq. (22) to the experimental signals with both $D_{\rm th}$ and Γ set as fitting parameters in addition to the scaling factor and baseline. The open squares (□) are the values obtained by fitting Eq. (22) with Γ fixed to 4.3×10^4 s^{-1}, which is the extrapolated value of Γ at 0 K, as described in the preceding section. The solid curve is an interpolation of the literature values of $D_{\rm th}$, which were estimated by combining the values of the thermal conductivity reported in Ref. 10 for parahydrogen-concentration of 99.66%, the specific heat at constant volume in Ref. 9, and the molar density of 0.0435 mol/cc. Note that the molar density is temperature independent in our experiment because our parahydrogen sample fills the sample cell and is not allowed to expand in the cell.[12] As seen in Fig. 9, the values represented by the closed circles (●) are approximately equal to the values represented by the open squares (□) at all temperatures except 7.2 K and 8.2 K. At these temperatures, however, the values represented by the closed circles (●) are singularly large. As we have mentioned in the preceding section, this is an artifact in the curve fitting processes. Therefore, we adopt the values represented by the open squares (□) as $D_{\rm th}$ for the temperatures 7.2 K and 8.2 K.

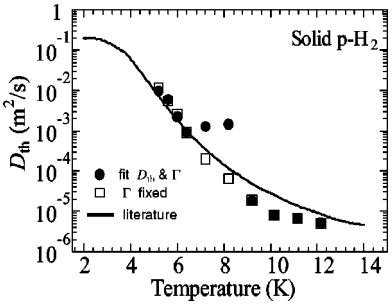

FIG. 9. Temperature dependence of the thermal diffusivity. The closed circles (●) represent the measured thermal diffusivity by fitting Eq. (22) with both $D_{\rm th}$ and Γ set as fitting parameters. The open squares (□) are the values obtained by fitting Eq. (22) with Γ fixed to 4.3×10^4 s^{-1}. The solid curve is an interpolation of the literature values of $D_{\rm th}$, which were calculated by combining the values of the thermal conductivity reported in Ref. 10 for parahydrogen-concentration of 99.66%, the specific heat at constant volume in Ref. 9, and the molar density of 0.0435 mol/cc.

The measured thermal diffusivity is almost consistent with the values estimated from literatures (the solid curve) below 7 K, while the literature values are slightly larger than the measured values between 7 K and 11 K. This can be explained qualitatively as follows. As has been pointed out,[12] the molar volume of solid parahydrogen rapidly increases approximately above 8 K. The parahydrogen samples employed previously could almost freely expand in the sample cell and would not experience any strong compression or strain at temperatures below the triple point, where these crystals were grown and the molar volume took the largest value.[10] In contrast, as the molar volume increases, our sample crystal experiences an increasing compression and strain because our parahydrogen sample fills the sample cell and cannot expand in the cell.[12] This additional strain should disturb the phonon propagation in the crystal to a greater extent than in the previous samples. Therefore, it is probable that the mean free path of phonons in our parahydrogen sample are shorter than that in the previous samples above 8 K, yielding smaller thermal diffusivity in this temperature range.

D. The mean free path of phonons and the hydrodynamic limit

If we assume isotropy, we can estimate the mean free path of phonons in the parahydrogen crystal from the relation

$$D_{\rm th}=\tfrac{1}{3}\overline{vl}, \tag{27}$$

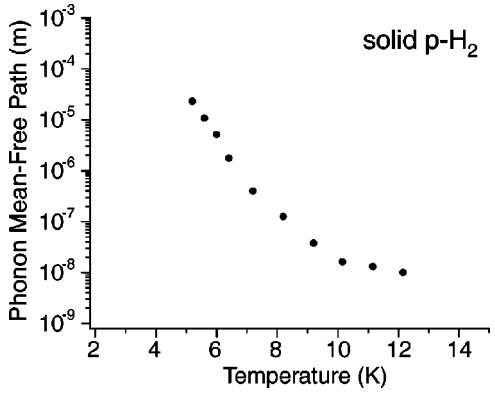

FIG. 10. The mean free path of phonons in solid parahydrogen of 99.7% orthohydrogen concentration estimated from the relation $\bar{l}=3D_{\mathrm{th}}/\bar{v}$. The mean velocity $\bar{v}$ is taken to be 1520 m/s.

where $\bar{v}$ and $\bar{l}$ are the mean velocity and mean-free path of phonons, respectively. We adopt Debye's mean velocity $[(1/v_l^2+2/v_t^2)/3]^{-1/2}$ as $\bar{v}$, where v_l and v_t are the longitudinal and transverse acoustic velocity, respectively, and we obtain $\bar{v}=1520$ m/s. As shown in Fig. 10, decreasing temperature lengthens the mean free path of phonons due to decrease in the number of the thermal phonons in the crystal.[25]

Next, we discuss the hydrodynamic limit to verify the validity of our macroscopic description made in Sec. II B. If $\bar{l}$ is sufficiently short compared to a characteristic length l_c, we can regard that the phonons collide frequently within the length l_c. In this case, the system can be treated as a gas of phonons, and such hydrodynamic or thermodynamic equations as Eqs. (4) or (5) are valid in a length scale longer than l_c. However, if the mean free path of phonons becomes comparable to or longer than l_c, local thermal equilibrium cannot be achieved within a length of l_c, and simple macroscopic descriptions cannot be applied to the system.[26–28]

If we take $\overline{q^{-1}}$ as l_c, the value $\overline{ql}$ corresponds to the inverse of the number of the phonon collisions within a length of $\overline{q^{-1}}$. For the achievement of local thermal equilibrium, therefore, we require that $\overline{ql}\ll 1$ at all temperatures that we investigated. We see in Fig. 10 that the value of $\bar{l}$ at the lowest temperature of 5.2 K is 23 μm, which gives $\overline{ql}\simeq 0.12$, indicating that approximately eight to nine collisions occur within a length of $\overline{q^{-1}}=w/2.40\simeq 200$ μm. This is a reasonably good condition for the achievement of local thermal equilibrium within the length scale of $\overline{q^{-1}}$, and our macroscopic description is actually valid at the lowest temperature investigated.

In general, we must be careful so that $\overline{ql}$ may not exceed unity when we apply the thermodynamic or hydrodynamic equations to a system of interest. Otherwise, the analysis may not be straightforward as done in this paper. Such a situation is possible when we cool the sample down to even lower temperatures, employ a smaller pump beam radius, or prepare a purer sample crystal (with higher parahydrogen concentration) which is known to make the phonon mean free path longer.[10] It is important to note that such discussions in terms of the value $\overline{ql}$ could not have been made without a concept of wave vector in thermal diffusion, while the concept has not been explicitly incorporated in the previous analyses on the TTLS.[8,14,15,18,19]

E. Discussions on the crossover temperature

Here we discuss on the ''crossover temperature,'' at which $D_{\mathrm{th}}\overline{q^2}$ becomes equal to Γ. We first consider the situation that $T=T_c$, where T_c is the crossover temperature. Since $\mathcal{T}_n(t)$ in Eq. (14) does not diverge even when $D_{\mathrm{th}}q_n^2=\Gamma$, nothing singular is expected to take place in the system at T_c except that the situation makes the fitting program unstable due to some $\frac{0}{0}$ problem in the curve fitting processes. If the contribution of a mode satisfying $D_{\mathrm{th}}q_n^2\simeq\Gamma$ is not so large, the curve fitting processes will not be affected so much. However, if the contribution of such a mode becomes larger, the fitting processes will be more influenced. The effect should be the largest when $D_{\mathrm{th}}\overline{q^2}\simeq\Gamma$ because the mode whose wave-vector magnitude is $\bar{q}$ has the largest contribution among the constituent modes in the TTLS signal, as have been already shown in Fig. 2. In fact, calculating D_{th} from the relation $D_{\mathrm{th}}=\Gamma/\overline{q^2}$ yields a D_{th} of 1.6×10^{-3} m^2/s, which lies between the values of D_{th} obtained for 6 K and 7 K (see Fig. 9). Although it is slightly lower than the temperatures such as 7 K or 8 K, this gives a good account of the artifact which appeared in the analysis for the temperatures around 7 K.

Next we consider the situation that $T<T_c$. According to Eq. (14), $\mathcal{T}_n(t)$ does not change its sign regardless of whether $D_{\mathrm{th}}q_n^2$ is greater or less than Γ. This means that a positive temperature change is always induced when $t>0$ even if the heat diffuses faster than it is created. In such a case, although it may sound paradoxical, the time dependence of the signal should now consist of a rising part due to thermal diffusion and a decay part due to heat creation. One may expect that no temperature rise occurs if heat diffuses faster than it is generated. However, Eq. (22) could not reproduce the experimental signals if we drop the modes which diffuse faster than the heat creation from the sum in the Eq. (22), i.e., if we assumed that $\mathcal{T}_n=0$ for n satisfying $D_{\mathrm{th}}q_n^2>\Gamma$. This implies that the experimental signals below T_c actually have rising rates faster than Γ. We consider that the nonsingular fitting results below 7 K shown in Figs. 8 and 9 also support the above discussion.

V. SUMMARY

We have measured the thermal diffusivity D_{th} and the nonradiative relaxation rates Γ for $\mathrm{Q}_1(0)+\mathrm{S}_2(0)$ and $\mathrm{Q}_2(0)+\mathrm{S}_1(0)$ transitions of parahydrogen molecule in the temperature range from 5.2 K to 12.2 K by using the technique of TTLS. To analyze the temporal evolution of the experimental signals, we have made a formulation which is suitable for our experimental conditions, i.e., we have assumed a small cylindrical sample cell and weak pumping energy. The solution obtained for the temporal evolution of the TTLS signal can be considered as a superposition of the

functions, each of which represents the temporal evolution of the TTGS signal with a finite signal rising time and various wave-vector components.

At temperatures higher than T_c, the signal rises at a rate of Γ and then decays at a rate of the thermal diffusion, while at temperatures below T_c, its vice versa. Here, T_c is the crossover temperature at which the average thermal diffusion rate $D_{\mathrm{th}}\overline{q}^2$ coincides with Γ. The values of D_{th} and Γ have been determined directly by fitting the derived function to the data in the temperature range from 5.2 K to 12.2 K. D_{th} has been found to be in good agreement with the previous measurements at low temperatures approximately below 8 K. The difference between our results and those from literatures above 8 K probably comes from the different method of sample preparation. We present in Table I the measured values of D_{th} in the temperature range from 5.2 K to 12.2 K.

Γ has been found to be almost temperature independent in the temperature range investigated, and its approximate value is 4.3×10^4 s^{-1}, which is substantially small compared to the value 3.0×10^5 s^{-1} reported by Kuo *et al.*[8] for the temperature of 11 K. This difference might be due to the uncertainties in the other temperature-dependent parameters such as dn/dT employed in their analysis.

Finally, we have introduced a characteristic wave-vector magnitude $\overline{q}$ in the TTLS. This parameter is particularly essential for the considerations on the local thermal equilibrium, which is associated with the relation between the mean free path of phonons and the characteristic length. We have also shown that $\overline{q}$ provides a quantitative comparison between the TTLS and TTGS for the first time to our knowledge.

Experiments should be carried out for lower temperatures in order to investigate the lattice anharmonicity of solid parahydrogen in detail. Effects of orthohydrogen concentration including the case of normal hydrogen crystal on the values of D_{th} and Γ also have to be studied. In addition, the temperature dependences for other excited states of hydrogen molecule should be explored. In carrying out these experiments, however, attention must be paid to the achievement of local thermal equilibrium, which can be verified from the relation between the mean free path of phonons and the characteristic length scale.

TABLE I. Temperature dependence of the thermal diffusivity of solid parahydrogen with parahydrogen concentration of 99.7% in the temperature range from 5.2 K to 12.2 K.

Temperature (K)	D_{th} (m^2/s)
5.2	1.2×10^{-2}
5.6	5.5×10^{-3}
6.0	2.6×10^{-3}
6.4	9.0×10^{-4}
7.2	2.0×10^{-4}
8.2	6.4×10^{-5}
9.2	1.9×10^{-5}
10.2	8.2×10^{-6}
11.2	6.6×10^{-6}
12.2	5.0×10^{-6}

ACKNOWLEDGMENTS

This work has been supported by CREST of Japan Science and Technology Corporation (JST).

[1] J.V. Kranendonk, *Solid Hydrogen* (Plenum, New York, 1983).
[2] T. Oka, Annu. Rev. Phys. Chem. **44**, 299 (1993).
[3] D.P. Weliky, T.J. Byers, K.E. Kerr, T. Momose, R.M. Dickson, and T. Oka, Appl. Phys. B: Lasers Opt. **B59**, 265 (1994).
[4] K. Kuroda, A. Koreeda, S. Takayanagi, M. Suzuki, and K. Hakuta, Phys. Rev. B **67**, 184303 (2003).
[5] K. Hakuta, M. Suzuki, M. Katsuragawa, and J.Z. Li, Phys. Rev. Lett. **79**, 209 (1997).
[6] J.Q. Liang, M. Katsuragawa, F.L. Kien, and K. Hakuta, Phys. Rev. Lett. **85**, 2474 (2000).
[7] M. Katsuragawa, J.Q. Liang, F.L. Kien, and K. Hakuta, Phys. Rev. A **65**, 025801 (2002).
[8] C.Y. Kuo, R.J. Kerl, N.D. Patel, and C.K.N. Patel, Phys. Rev. Lett. **53**, 2575 (1984).
[9] G. Ahlers, J. Chem. Phys. **41**, 86 (1964).
[10] P.C. Souers, *Hydrogen Properties for Fusion Energy* (University of California, Berkeley, 1986).
[11] F.L. Kien, A. Koreeda, K. Kuroda, M. Suzuki, and K. Hakuta, Jpn. J. Appl. Phys., Part 1 **42**, 3483 (2003).
[12] M. Suzuki, M. Katsuragawa, R.S.D. Sihombing, J.Z. Li, and K. Hakuta, J. Low Temp. Phys. **58**, R58 (1998).
[13] K.A. Nelson, R.J.D. Miller, D.R. Lutz, and M.D. Fayer, J. Appl. Phys. **53**, 1144 (1982).
[14] J.P. Gordon, R.C.C. Leite, R.S. Moore, S.P.S. Porto, and J.R. Whinnery, J. Appl. Phys. **36**, 3 (1965).
[15] R.L. Swofford and J.A. Morrel, J. Appl. Phys. **49**, 3667 (1978).
[16] J.R. Barker and T. Rothem, Chem. Phys. **68**, 331 (1982).
[17] R.K. Wehner and R. Klein, Physica (Utrecht) **62**, 161 (1972).
[18] J.R. Whinney, Acc. Chem. Res. **7**, 255 (1974).
[19] J.Z. Li, M. Suzuki, M. Katsuragawa, and K. Hakuta, J. Chem. Phys. **115**, 930 (2001).
[20] D.A. Long, *Raman Spectroscopy* (MacGraw-Hill, New York, 1977).
[21] M. Mengel, B.P. Winnewisser, and M. Winnewisser, J. Mol. Spectrosc. **188**, 221 (1998).
[22] A. Nitzan and J. Jortner, Mol. Phys. **25**, 713 (1973).
[23] A. Nitzan, S. Mukamel, and J. Jortner, J. Chem. Phys. **60**, 3929 (1974).
[24] A. Nitzan, S. Mukamel, and J. Jortner, J. Chem. Phys. **63**, 200 (1974).
[25] C. Kittel, *Introduction to Solid State Physics* (Wiley, New York, 1953).
[26] A. Koreeda, M. Yoshizawa, S. Saikan, and M. Grimsditch, Phys. Rev. B **60**, 12 730 (1999).
[27] H.E. Jackson, R.T. Harley, S.M. Lindsay, and M.W. Anderson, Phys. Rev. Lett. **54**, 459 (1985).
[28] P.R. Stoddart and J.D. Comins, Phys. Rev. B **62**, 15 383 (2000).